The STAR Detector Magnet Subsystem

F. Bergsma [a], C.O. Blyth [b], R.L. Brown [c], W. Dieffenbach [c], A. Etkin [c], K.J. Foley [c], P.-A. Giudici [a], W.J. Leonhardt [c], W. Love [c], J.A. Mills [c], D. Phillips [c], I. Polk [c], E.S. Roger [c], P. Rosas [c], J. Sandberg [c], J.A. Scheblein [c], R.D. Schlueter [d], F. Toldo [c], S. Trentalange [e], H. Wieman [d]

[a] *CERN, Geneva, Switzerland*

[b] *University of Birmingham, Birmingham, United Kingdom*

[c] *Brookhaven National Laboratory, Upton, NY 11973*

[d] *Lawrence Berkeley Laboratory, Berkeley, California 94720*

[e] *University of California at Los Angeles, LA, CA 90095*

Abstract

We describe the specification and design, construction and mapping of the STAR magnet. Measurements demonstrate that field quality exceeds specifications for uniformity and agrees with design values.

1 Design Considerations

A Time Project Chamber (TPC) lies at the heart of the STAR detector. The TPC is a large cylindrical tracking device for charged particles covering a coordinate range -210 cm$< z <$+210 cm, 50 cm$< r <$200 cm and $0 < \phi < 2\pi$. It is divided into two halves (East and West) by a central membrane at $z = 0$ with the electric fields in each half pointing in opposite directions. The TPC produces an image of all charged particle tracks passing through the detector. These tracks consist of finely-spaced clusters of ionization which drift under the influence of a nearly uniform electric field to planes of electronics located at each end of the cylinder. The drift distance refers to the difference between the point of ionization, z, and the detector planes of the TPC, which are located at $z = \pm 210$ cm. The accuracy of space point reconstruction from which the particle momenta and trajectories are determined depends on detailed knowledge of the electric and magnetic fields.

The physics goals of STAR lead to a set of requirements on the strength and precision of the magnetic field. A primary restriction comes from momentum mea-

surements of high-energy electron tracks, which are nearly straight. However, all clusters drift through part of the magnetic field. Hence the field homogeneity requirement was determined by combining the tracking accuracy requirement for high energy electrons (~ 200 μm), with estimates of the position reconstruction accuracy due to uncertainties in the magnetic field (~ 0.5 Gauss). The homogeneity specifications are expressed in terms of the following integrals:

$$|\Im_r| \equiv \left| \int_{z'=210\ \mathrm{cm}}^{z} (B_r/B_{z'}) dz' \right| \ \leq \ 7.0\ \mathrm{mm}$$

$$|\Im_\phi| \equiv \left| \int_{z'=210\ \mathrm{cm}}^{z} (B_\phi/B_{z'}) dz' \right| \ \leq \ 2.5\ \mathrm{mm}$$

These integrals are related to the drift distortions, but do not include factors relating to properties of the TPC gas or Electric field direction. These are discussed in more detail in the description of the TPC and in Ref. [1].

Further design constraints are the requirement of sufficient space inside the coils for an electromagnetic calorimeter, apertures in each poletip to allow particle transmission at psuedorapidity $|\eta| > 2.0$ (for external trigger and luminosity detectors) and space between each coil to route fiber bundles for the external electronics of the EMC. A cross section of the magnet steel and coil geometry is given in Figure 1.

The magnet system was designed by R.D. Schlueter of Lawrence Berkeley Laboratory[2]. The optimal design incorporates correction coils located on the poletips as well as trim coils located in line with the main coils. The final design produces a near uniform field over the operating range $0.25 < |B_z| < 0.5$ T with an estimated uniformity of $|\Im_r| \leq 2.3$ mm and $|\Im_\phi| \leq 1.0$ mm over the entire TPC volume. Note that the TPC only fills a fraction of the inner field volume.

2 Magnet Steel Design

The magnet steel functions as the return flux path for the field and also as the support structure for the internal and external detector elements. The magnet is roughly cylindrical in geometry and consists of 30 flux return bars (backlegs), four end rings and two poletips. The 6.85 m long flux return bars are trapezoidal in cross section and weigh 18 tons each. They form the outer wall of the cylinder which encloses the main and space trim coils and are attached to an inner and outer end ring pair at each end of the magnet. The inner end rings have an inner diameter of 5.27 m with 30 chord surfaces on the 6.28 m outer diameter to fix the azimuth location of each flux return bar. Each inner ring has an axial thickness of 285 mm and weighs 25 tons. The outer rings are the structural connection between the ends of the flux return bars and have the same I.D. as the inner rings with a 7.32 m O.D. and 203 mm axial thickness, weighing 35 tons each. Each poletip weighs 73 tons

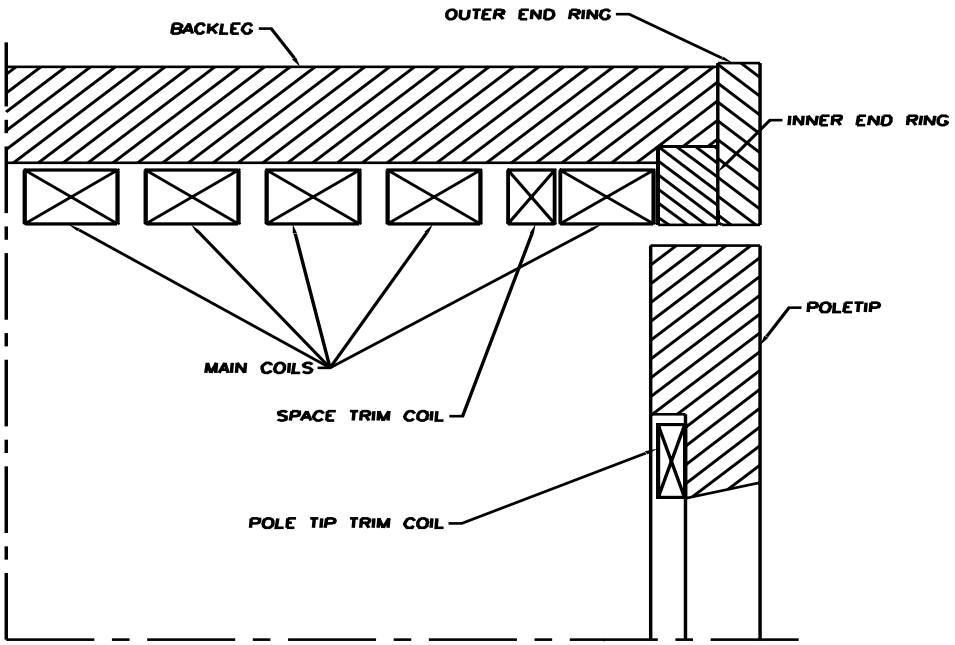

Fig. 1. Section drawing of magnet steel and coil locations. Dimensions are given in the text.

and is on axis with and supported by the end rings. Each poletip has a conical I.D. at $\eta = 2$ with a 525 mm axial thickness, a 5.06 m O.D. and a counterbore on the inner face for the pole tip trim coil. There is a 107 mm annular gap between the end ring I.D. and the poletip O.D. for utility routing to internal detector elements.

The above elements, weighing 1100 tons, rest on two 36 ton cradles which cover the bottom 9 backlegs. These cradles, in turn, rest on Hillman Rollers and hydraulic pistons which are guided by rails between the assembly building and experimental hall. Each of the poletips has a 100 ton support carriage allowing independent removal of each poletip using hydraulic jacks. The poletip support carriages were fabricated and assembled by Ranor Inc., Westminster, MA. The hydraulic systems for manipulation of both the main magnet and the poletip support carriages were supplied by Atlantic Fluid Power, Hauppauge, NY. All magnet yoke material is AISI 1008 killed steel that is vacuum degassed with fully annealed heat treatment resulting in a minimum yield strength of 172 MPa. The support structure was constructed of steel with ASTM A36 specification. The details of the magnet construction have been given previously in Ref. [3].

To maintain magnetic field quality, deflections in the magnet structure are minimized to less than 1 mm. The magnetic components were precision fabricated and mating connections used high-strength bolts and pinned connections. The prime contractor for fabricating the magnet steel was Precision Components Corp., York, PA. Materials for the magnet yoke (flux return bars and end rings) were procured from Creusot-Marrel, France, while the poletips were procured from Japan Steel Works, Japan. All components were provided as single piece forgings except for the outer end rings which were formed from four flame-cut arcs of flat rolled steel, then

electroslag welded together to form each ring. Final fabrication of each component was performed at either PCC or their subcontractor Gec Alsthom, Canada. End ring pairs were aligned and match pinned to insure accurate assembly and structural integrity. High strength threaded inserts were used in this low yield strength material, along with expansion bolts, torque bolts and mechanical tensioners from Superbolt Corp, Carnegie, PA. Use of these high strength fasteners allowed us to achieve the fixed end bolted connections needed to minimize deflection of the steel structure with accurate bolt tension using standard hand-held torque wrenches. This also eliminated the need for anchor points in the steel to support much heavier mechanical or hydraulic torque wrenches used on standard hex-head fasteners.

3 Coil Design

There are three types of magnet coils: Main, Space Trim and Poletip Trim. The Main and Space Trim coils were fabricated by Tesla Engineering Ltd of Storrington, UK; while the Poletip Trim coils was fabricated by Everson Electric of Bethlehem, PA. Each coil assembly was constructed from hollow rectangular aluminum conductor, insulated with fiberglass cloth and vacuum-impregnated with epoxy.

The Main and Space Trim coils are built from two layer pancakes wound two-in-hand (bifilar) fashion in 13 turns. The nominal dimensions for these coils are 5.3 m I.D. by 6.0 m O.D. with an axial thickness of 0.45 m for the Main Coils and 0.23 m for the Space Trim coils. The pancakes are wound in both a right-handed and left-handed sense and stacked alternately to cancel off-axis field components from the layer-to-layer winding transitions. The conductor for these coils measures 53.9 mm by 47.5 mm with a 16.8 mm diameter central round hole for cooling water circulation. Each pancake contains two parallel water circuits approximately 120 m in length.

The magnet contains ten Main coils with four pancakes each and two Space Trim coils containing two pancakes each. These coils are connected in series electrically, while the (88) cooling water circuits are connected in parallel. At the maximum field of 0.5 T, the current through these coils is 4500 A, with an additional 12-13% current through the Space Trim coils. Total power consumption is 3.5 MW.

Each poletip includes a trim coil to help attain magnetic field uniformity. The Al conductor for these coils measures 22.2 mm square with a 12.3 mm diameter central water hole. The coils contain six layers, wound three-in-hand (trifilar) fashion giving 118 turns per coil. Every two layers contains three separate water circuits giving a total of nine circuits per coil. Water circuits are approximately 95 m long. Each coil is 1.8 m I.D. by 2.8 m O.D. with an axial thickness of 0.14 m and weighs approximately 1.2 tons. The current through the Poletip coils is 1330 A at maximum field.

The magnet water cooling system is a closed-loop system with a flow rate of 1200 GPM through heat-exchangers. These in turn are cooled by an open loop water system with cooling tower. The closed-loop system (supply temp = 24°C, return temp = 29°C, pressure = 200 PSI) dissipates approximately 3.5 MW of power in order to keep the magnet coils operating at a mean temperature of 29 °C. Because the coils are fabricated from aluminum, it is important to minimize corrosion or electrolytic effects on the conductor. The only metals used in the water system are stainless steel or aluminum. Resin-bed dionizers and oxygen scavengers maintain the resistivity of the water to > 5 MΩ-cm and the dissolved oxygen levels to < 0.1 ppm. The magnet has been in operation for 2 years with no observed corrosion problems.

4 Power Supplies

As shown in Figure 2, there are five separate power supplies required for proper magnetic field shaping. The main magnet power supply delivers positive and negative voltages, which, because of the center feed, gives a virtual ground at the endcaps. This reduces possible pickup of ripple by the TPC electronics and also lowers the standoff voltage requirements of the booster supplies. Due to the balanced nature of the power supply loads, the ground potential on the main supply is midway between the output terminals. Except for the boosters, the power supplies are separated into two parts, transformers (from NWL, Inc., Bordentown, NJ) and rectifier control sections (from Macroamp, Ukiah, CA). The boosters were purchased as complete packages from Inver Power Controls, Ltd.

A Programmable Logic Controller monitors magnet performance and gives automatic shut-down capability. In order to protect against over-heating after a loss of cooling water or blockage, a thermister is attached at the output end of each water path. If any thermister reading exceeds the maximum allowed temperature the magnet currents are run down over a period of 2 minutes; if the temperature continues to rise, the power supplies are shut down. This relatively slow rampdown minimizes stress on the entire sysem while ensuring fail-safe protection. In addition, the voltage across each individual conductor is monitored to detect turn-to-turn shorts. Again, the power supplies are run down when a possible fault is detected.

5 Magnetic Field Optimization

Field optimization (tuning of the trim/poletip currents) and calibration of the absolute magnetic field were initially performed using an NMR probe which was moved along the central axis. The excitation function of the main coil and each trim and

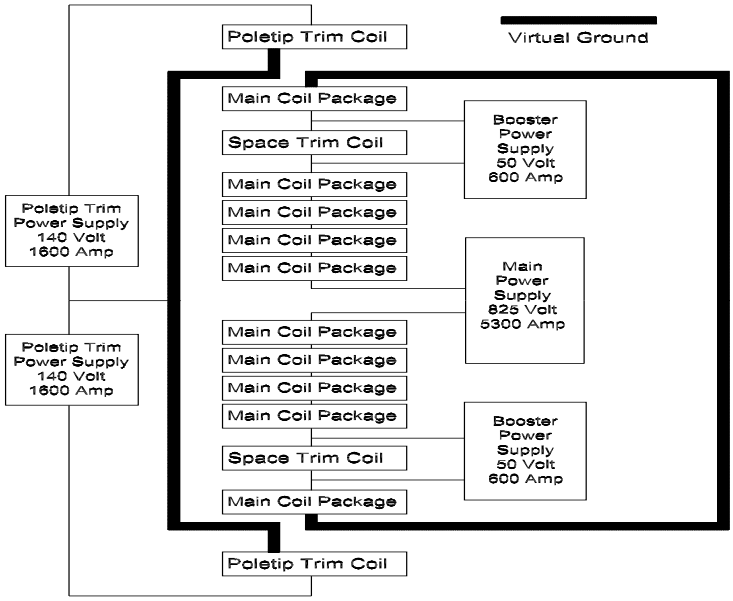

Fig. 2. Power supply connections for the STAR Magnet.

pole tip coil was separately determined at values near their nominal settings in order to minimize the nonlinear effects of saturation in the steel. The optimal settings were then computed by minimization of the axial field variations with respect to these currents. Partial maps were taken with the mapper arms set at $\phi = 0^{\rm o}$ and $90^{\rm o}$ to confirm the optimum setting by direct variation around the computed minima.

The stabilization of the field due to all effects (temperature, power supply settling, etc.) takes approximately 10-20 seconds. The reproducibility of the absolute field was better than $\pm$0.5 Gauss. The central positive and negative fields are the same magnitude to better than 0.25 Gauss for both full and half field settings. Long-term drift of the field was measured to be $\pm$0.1 Gauss over a period of 12 hours.

6 Magnetic Field Mapping

A full field map consists of measurements of all three components B_r, B_ϕ, B_z at 14 radial points, 36 azimuthal points ($\Delta\phi = 10^{\rm o}$) and 57 axial locations ($\Delta z =$ 10 cm) covering a cylindrical volume with a radius of about 230 cm and length of 5.6 m. Thus, the measured maps consisted of points equally spaced in ϕ and z and roughly equal in r. We used an existing apparatus, available from CERN, consisting of a steerable array of Hall probes, supplemented by NMR measurements for normalization and cross-check purposes. This was designed and built by MPI-Munich in collaboration with CERN. This device has a central axis mounted on a bridge which moves along two rails $>$6 m long mounted on opposite sides of the inner diameter of the magnet. with two rotating arms 2.4 m in radius. Each arm holds an

array of 14 measuring heads containing 2 Hall probes for each component, making a total of 2 x 3 x 14 x 2 = 168 Hall plates. Two stepping motors with encoders move the arms in the ϕ and z directions, so the whole field can be mapped automatically. A complete map was taken as a series of z planes. At each z plane, the mapper was stepped a complete $360^{\rm o}$ in $10^{\rm o}$ ϕ intervals. Overlap points were taken to establish the consistency of the data, especially where the mapper had to be repositioned. The final grid size was chosen after careful study of more detailed partial maps for small-scale variations: down to $\Delta z = 1$ cm and $\Delta\phi = 1^{\rm o}$. The mapping device was surveyed both before and after the magnet mapping using a MANCAT system. Using the results of this survey, the rotating arms can be positioned at any point along the axis to $\pm$0.2 mm absolute accuracy. Both carriage positions are separately encoded to an accuracy of about $\pm$0.3 mm. The arms can be turned through 360 degrees with an accuracy of 0.75 mrad (25 encoder counts/degree).

The Hall elements themselves are Siemans Model SBV 579 Indium Arsenide cruciform Hall plates, with an active area of about 1.6 mm on each side. The sensitivity is about 130 mV/T, with typical signals of less than 60 mV. These signals were read out with a 5 1/2 digit Hewlett-Packard voltmeter with a low noise multiplexer. This multiplexer was found to have a warm-up time of several days; it was, therefore, never switched off. The Hall probes, voltmeter and multiplexer were kept powered without interuption for 3 months prior to these measurements. During the reversal of the mapper orientation during the last few days of the measurement period, it was necessary to switch off the Hall probes and voltmeter for one day. The multiplexer was left powered up. The stabilization time of the Hall probes alone was observed to be less than 5 hours.

The Hall probes were not temperature-controlled. The largest source of random error in these measurements was the thermal drift of the Hall coefficient and offset voltages. Typical values for these quantities were $V_{\rm o} = 100$ μV for the offset voltage and $K = 130$ mV/T for the Hall coefficient. The thermal coefficients for these quantities were approximately $(\Delta V_{\rm o}/V_{\rm o})/\Delta T = 1.5\ 10^{-2}\ (^{\rm o}{\rm C})^{-1}$ and $(\Delta K/K) = -4.0\ 10^{-4}\ (^{\rm o}{\rm C})^{-1}$. These corrections were applied to the data. The absolute calibration accuracy of the Hall probes was ± 3 Gauss; however, repeated tests both at CERN and BNL established the short-term fluctuations for these probes to be $\pm$0.035 Gauss for an individual measurement.

The main component, B_z, was measured directly. This component is insensitive to slight angular misalignments of the Hall probes with respect to the z axis of the magnet. The relative accuracy of the map is improved to $\pm$0.2 Gauss by fitting a smooth function through portions of the map where the field is slowly varying and subtracting individual Hall probe offsets from the entire map. The Hall probe measurements near the magnet axis were cross-calibrated against an NMR probe in the same z plane.

The radial and phi components were measured directly, but corrected for misalign-

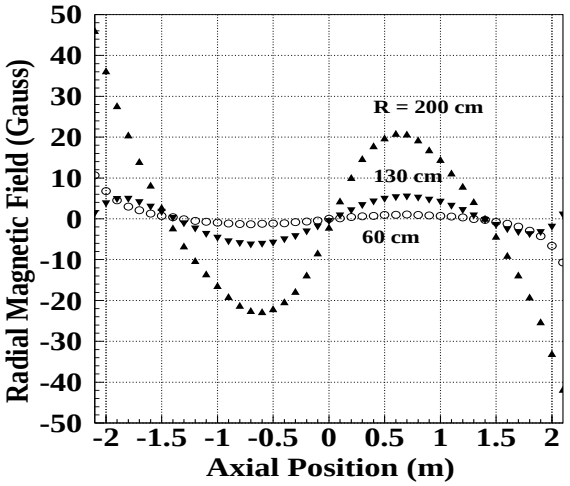

Fig. 3. Measurements of radial component of the STAR magnetic field (Gauss) as a function of axial (z) position for three radii at $\phi = 0^o$. The center of the TPC and the magnet are at $z = 0$. The inner and outer radii of the TPC are 50 cm and 200 cm, respectively.

ments with the z axis of the magnet as well as the axis of rotation of the mapping device. The first effect is removed by subtracting offsets in the same manner as the B_z component. The misalignment of the individual probes with the mapper rotation axis were subtracted by determining the amplitude of the variation as a function of ϕ angle. This was determined independently for each arm using the variation of the innermost two probes as a function of ϕ at each z plane. This variation was subtracted from all the radial probes on each arm for each ϕ angle. The validity of this procedure depends on the fact that the variation of the innermost r and ϕ probes is less than $\pm$0.2 Gauss. This was established from the variation of B_z and B_ϕ and determining the r component by integrating $\nabla \cdot B = 0$, assuming $B_r = 0$ at the center of the magnet.

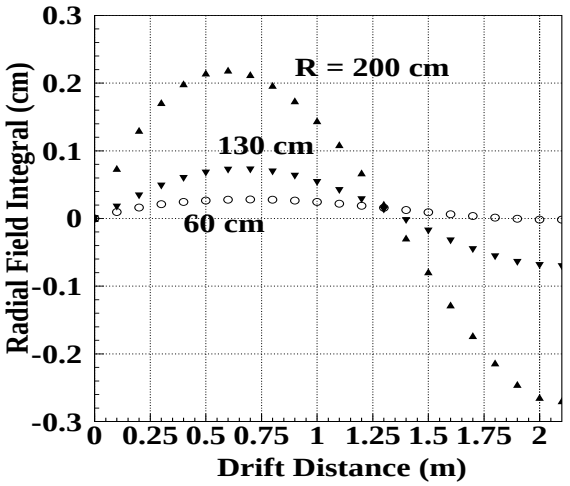

Fig. 4. Values of the field integral ($\Im_r$) of the STAR magnetic field (cm) as a function of drift distance. Representative data are given at three radii in the TPC for $\phi = 0^o$ and $z < 0$ (TPC East Half).

7 Field Measurements and Distortion Integrals

Complete field maps were taken at full field positive and negative, as well as at half field positive. A nearly complete map was taken at half field negative. Due to independent trim coil optimization, the half field maps are slightly different in shape than the full field maps, especially away from the magnet center. The maximum excursion of the radial component for full(half) field is approximately ± 50 Gauss (± 25 Gauss). The ϕ component of the field is less than ± 3 Gauss (± 1.5 Gauss) . In Figure 3 we plot typical results for the radial field component as a function of axial position for three radii within the TPC.

In Figure 4 we plot the corresponding field integrals $\Im_r$ for these same three field measurements. The results at angle $\phi = 0^o$ are typical, however there is also an angular variation of the radial field. Within the volume of the TPC, the maximum variation of the field integrals is $|\Im_r| < 0.30$ cm and $|\Im_\phi| < 0.035$ cm. This is a factor of 2 better than the specifications and in agreement with the design calculations.

References

[1] H. Wieman, STAR Note #14 which is available at http://www.star.bnl.gov

[2] R.D. Schlueter, LBL Internal Report.

[3] R.L. Brown et al., Proc. of the IEEE 1997 Particle Accelerator Conference (1998) 3230 .